J Solid State Electrochem (1998) 2: 308–314

ORIGINAL PAPER

Aleksey A. Yaremchenko · Vladislav V. Kharton
Evgeny N. Naumovich · Anneta A. Tonoyan
Viktor V. Samokhval

Oxygen ionic transport in Bi_2O_3-based oxides: II. The Bi_2O_3–ZrO_2–Y_2O_3 and Bi_2O_3–Nb_2O_5–Ho_2O_3 solid solutions

Received: 31 October 1997 / Accepted: 18 December 1997

Abstract Electrical conductivity, fluorite-type cubic unit cell volume and thermal expansion of the $(Bi_{1-x}Nb_x)_{1-y}Ho_yO_{1.5+\delta}$ ($x = 0.05$ and 0.08; $y = 0.10-0.15$) and $(Bi_{1-x}Zr_x)_{1-y}Y_yO_{1.5+\delta}$ ($x = 0.05$ and 0.07; $y = 0.15$) solid solutions have been found to decrease regularly with increasing dopant content. Annealing at temperatures below 900 K leads to a phase decomposition and to a sharp decrease in conductivity of the ceramics. Oxygen ion transference numbers have been determined by the e.m.f. method and by Faradaic efficiency measurement to exceed 0.9. A new technique of studying Faradaic efficiency has been proposed and verified using $(Bi_{0.95}Zr_{0.05})_{0.85}Y_{0.15}O_{1.5+\delta}$ and $Zr_{0.90}Y_{0.10}O_{1.95}$ ceramic samples.

Key words Oxygen ionic conductivity · Bismuth oxide · Transference numbers · Faradaic efficiency · Thermal expansion

Introduction

Ceramic materials on the basis of stabilized δ-Bi_2O_3 having high oxygen ionic conductivity are promising solid electrolytes for high-temperature oxygen pumps, fuel cells and sensors. An important application of the Bi_2O_3-based oxides is dual-phase oxygen membranes for oxygen separation, which represent a mixture of an electronic conductor phase and an ionically conducting oxide phase [1–3]. Metallic silver, palladium, oxides of cobalt, copper and iron and bismuth cuprate $Bi_2CuO_{4-\delta}$ have been tested as the electronically conductive second phase in the dual-phase membranes [4–9]. It has been ascertained that the oxygen ionic transference number of the $Bi_{0.75}Y_{0.25}O_{1.5}$–$Bi_2CuO_{4-\delta}$ ceramics is comparable with the electronic one at 920 K when the bismuth cuprate phase concentration is about 30 vol% [9]. Analogous results were obtained from the numerical calculations using a resistor network approach for the silver and nickel metal phases as the electronic conductor [3].

The disadvantages of the electrolytes derived from bismuth oxide are a transformation of the δ-Bi_2O_3 phase into a rhombohedral phase and a formation of superstructures at temperatures below 900 K [10–13]. The structure changes may lead to a sharp decrease in conductivity. Additions of ZrO_2 and CeO_2 into the ceramics have been shown to suppress this decay [13, 14].

A number of our previous research projects [15–19] have been devoted to studying solid electrolytes and mixed-conducting ceramics on the basis of stabilized δ-Bi_2O_3 in the oxide systems Bi_2O_3–Y_2O_3–Pr_6O_{11}, Bi_2O_3–Co_3O_4–Y_2O_3, Bi_2O_3–PbO–Y_2O_3, Bi_2O_3–ZrO_2–Y_2O_3 and Bi_2O_3–Y_2O_3. The order in which the components are added in the course of preparation has been demonstrated to affect the phase composition and transport properties of Bi_2O_3-containing materials in the ternary oxide systems. Introduction of a less soluble component and synthesis of binary solid solutions with subsequent addition of a more soluble component is a promising method to prepare Bi_2O_3-based electrolytes with two dopants [15, 16].

The aim of the present work was to investigate transport properties of the $Bi(Zr,Y)O_{1.5+\delta}$ and $Bi(Nb,Ho)O_{1.5+\delta}$ fluorite-type solid solutions.

Experimental

Preparation and characterization

A two-stage standard ceramic synthesis route was used to prepare $(Bi_{1-x}Nb_x)_{1-y}Ho_yO_{1.5+\delta}$ ($x = 0.05$ and 0.08; $y = 0.05 - 0.15$) powders. In the first stage, $Bi_{1-x}Nb_xO_{1.5+\delta}$ ($x = 0.05$ and 0.08) were

A.A. Yaremchenko · V.V. Kharton (✉) · E.N. Naumovich · A.A. Tonoyan · V.V. Samokhval
Institute of Physicochemical Problems, Belarus State University, 14 Leningradskaya Str., 220080, Minsk, Republic of Belarus
Tel.: +375-17-2207681; Fax: +375-17-2264696;
e-mail: kharton@fhp.bsu.unibel.by or nen@basnet.minsk.by

synthesized using high-purity $Bi(NO_3)_3 \cdot 5H_2O$ and Nb_2O_5 as starting materials. The solid-state reactions were conducted in air at temperatures of 1020–1080 K for 15–20 h with multiple repeated intermediate grindings. At the second stage of the synthesis, holmium oxide (99.99%), which had been previously annealed at 1300 K for 5–6 h, was added to the mixtures. Then the mixtures were subjected to annealing at 1050–1130 K for 20–25 h with the intermediate grindings. Ceramic specimens were pressed (200–600 MPa) in the shape of bars ($4 \times 4 \times 30\,mm^3$) and disks of various thickness (diameter 12 or 15 mm). The gas-tight ceramics were sintered in air at 1180–1210 K for 20–40 h.

The two-step synthesis procedure used for the preparation of $(Bi_{1-x}Zr_x)_{1-y}Y_yO_{1.5+\delta}$ ($x = 0.05$ and 0.07; $y = 0.15$) was analogous. As the starting materials of the first stage, we used high-purity $Bi(NO_3)_3 \cdot 5H_2O$ and $ZrO(NO_3)_2 \cdot 2H_2O$. Yttrium nitrate $Y(NO_3)_3 \cdot 6H_2O$ was added after annealing the Bi_2O_3–ZrO_2 starting mixtures at 920–1040 K for 30–40 h. The solid-state reactions of the second stage were conducted in air at 1100–1150 K with 15–20 h multiple repeated intermediate grindings. The gas-tight ceramic specimens were sintered at 1240 ± 10 K for 20–30 h in atmospheric air.

The powders and ceramics of $(Bi_{1-x}Nb_x)_{1-y}Ho_yO_{1.5+\delta}$ and $(Bi_{1-x}Zr_x)_{1-y}Y_yO_{1.5+\delta}$ were characterized by X-Ray diffraction (XRD), X-Ray fluorescence analysis (XRF), atomic emission spectroscopy (AES) and differential thermal analysis (DTA). The experimental procedures of XRD, XRF, AES, DTA, in the study of thermal expansion and electrical conductivity have been described elsewhere [16–21].

The e.m.f. measurements

The technique used to determine oxygen ion transference numbers (t_o) by a modified e.m.f. method has been described in [17, 22]. The transference numbers of the gas-tight ceramics were measured using the concentration cell:

$$O_2(p_{O_2} = 1.01 \times 10^5\,Pa),\ Ag|Oxide|Ag,\ O_2(p_{O_2} = 0.21 \times 10^5\,Pa) \quad (1)$$

In order to estimate the transference parameters at lower oxygen partial pressures, we also studied the cell

$$O_2(p_{O_2} = 0.21 \times 10^5\,Pa),\ Ag|Oxide|Ag,\ O_2(p_{O_2} = 16\,Pa) \quad (2)$$

As the oxygen partial pressure gradient is excessively large in the case of cell 2, the values of t_o determined using this cell represent only a qualitative estimation [23, 24]. During the investigations, corresponding gases (oxygen, air or nitrogen) were supplied into the electrode volume continuously in order to maintain steady oxygen chemical potentials at the electrodes. Oxygen concentration in the nitrogen flux was measured using a Zirkon-M gas-analyzer. A modification of the e.m.f. method proposed by Gorelov [17, 22] was used to eliminate any effect of the electrode polarization resistance on the ion transference number value measured.

The Faradaic efficiency studies

The oxygen ion transference numbers were also calculated from the Faradaic efficiency measurement results. For these measurements, we used an electrochemical cell presented in Fig. 1 and described below. The use of such a cell was necessitated by the considerable limitations of other known techniques to determine the Faradaic efficiency [25–27]. For instance, the first of the known techniques is based on the analysis of oxygen concentration in the inert carrier gas flux which flows over the anode of a studied electrochemical cell [25, 26]. Here oxygen is pumped through the electrolyte specimen into the carrier gas flux as a result of an electrical potential difference applied to the electrodes. The transference number can be calculated from the ratio between the oxygen flux and the direct current passed through the cell [25, 26]. For the Bi_2O_3-based materials, a possible limitation of this method is associated with difficulties in determining oxygen leakage flux, which could be caused by orginating electronic conductivity due to the electrolyte reduction. As the electronic conductivity depends on both oxygen partial pressure and the electrode overpotential, the oxygen permeation flux value measured when the electrical current through the cell is equal to zero ($I = 0$) may be different from the permeation flux when $I \neq 0$. In this case, one could expect increasing experimental error in the ion transference number values determined by this method.

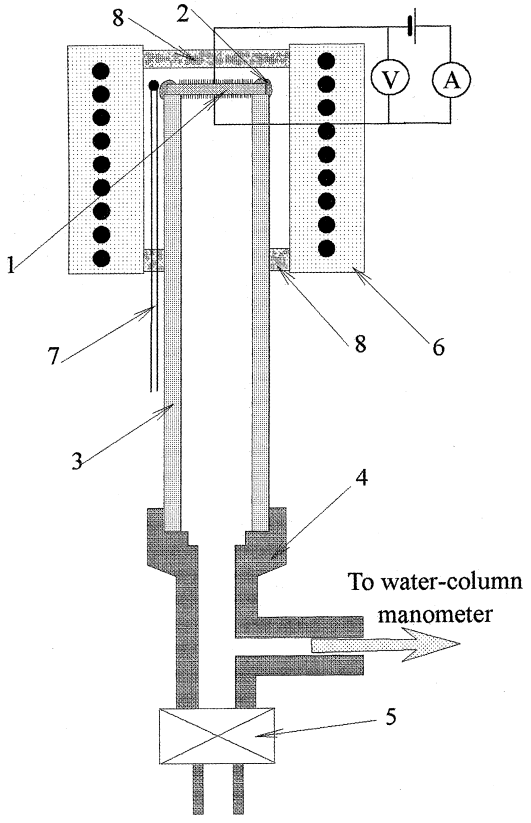

Fig. 1 The measurement cell for the Faradaic efficiency studies: *1* ceramic specimen with metal electrodes, *2* high-temperature sealant, *3* YSZ tube, *4* metallic construction, *5* valve, *6* furnace, *7* thermocouple, *8* high-porosity ceramic insertions

The second technique has been described in one of our previous papers [27]. In the framework of this method, oxygen is pumped through a specimen into a yttria-stabilized zirconia (YSZ) cell and simultaneously removed from the cell by an electrochemical pump. The currents through the specimen and through the pump are chosen to provide an oxygen chemical potential in the internal volume of the cell to be close to the external oxygen chemical potential. When a steady state is achieved, the transference numbers are determined by the ratio between the currents. However, the measurement cell made of YSZ could not be used at temperatures below 900 K.

A schematic drawing of the cell used for studying Faradaic efficiency in the present work is shown in Fig. 1. A gas-tight ceramic specimen with porous electrodes of metallic silver was hermetically sealed to a dense YSZ tube. The current collectors of the cell were made of platinum. The cell was connected to a standard water-column manometer. Before each measurement cycle, atmospheric air was blown through the cell. In the course of

measurement a direct current was passed through the cell to pump oxygen into the internal volume. The current value was kept constant with an accuracy of 0.2%. The measured quantities were as follows: increments of pressure and volume as a function of time, the voltage between the electrodes, atmospheric pressure, temperatures of the heated and cold parts of the device.

The oxygen flux density $j_o(t)$ (mol s^{-1} cm^{-2}) pumped through the specimen is defined by the equation:

$$j_o(t) = S^{-1} \cdot \left[\frac{dv_o(t)}{dt}\right] \quad (3)$$

where S(cm^2) is the electrode surface area, v_o (mol) is the amount of oxygen pumped into the cell and t is the time after starting the measurement cycle. The quantity v_o was calculated from the water-column manometer reading with consideration of the atmospheric pressure and temperature of the system. The measurements were performed at temperatures from 770 to 1100 K and the direct current densities up to 150 mA cm^{-2}. Total time of the measurement cycle was varied from 1 to 3 h, whereas the difference of oxygen partial pressures at the electrodes was 0–4 $\times$ 10^3 Pa.

The oxygen ion transference is proportional to the ratio between oxygen flux and total electrical current through the cell [28]:

$$t_o = \frac{4FS \cdot j_o(t)}{I(t)} \quad (4)$$

where I is the intensity of the direct current through the cell.

Pumping oxygen into the cell results in increasing oxygen partial pressure at the anode, which may lead to a change in the transference numbers. The oxygen ion transference number in air can be determined only in the initial stage of the experiment while oxygen pressures at electrodes are sufficiently close to each other. In this case, a linear relationship between the charge passed through the specimen and the amount of oxygen is observed:

$$4F \cdot v_0(\tau) = t_0 \cdot Q(\tau) = t_0 \cdot \int_{t=0}^{t=\tau} I(t)\, dt \quad (5)$$

where $Q(\tau)$ is the total charge passed between electrodes at the instant τ.

In the present work, the oxygen ion transference number in air was calculated using the linear fitting model:

$$4F \cdot v_o(\tau) = A + t_o \cdot Q(\tau) \quad (6)$$

where A and t_o are the regression parameters ($A \approx 0$). As a rule, the parameter A, which is determined by the experimental error, was statistically insignificant. Each set of the experimental values for the fitting was selected subject to the condition $\tau \to 0$ in order to provide a maximum adequacy of the model.

The described technique of studying Faradaic efficiency was verified using dense ceramic specimens of $Zr_{0.90}Y_{0.10}O_{1.95}$ with platinum electrodes. Within the limits of experimental error, the oxygen ion transference numbers of YSZ were calculated to be equal to 1.00, as one would expect. The experimental error of the YSZ transference number determination was estimated to be approximately 0.03.

Results and discussion

XRD studies demonstrated that all as-prepared powders and ceramics of $(Bi_{1-x}Nb_x)_{1-y}Ho_yO_{1.5+\delta}$ and $(Bi_{1-x}Zr_x)_{1-y}Y_yO_{1.5+\delta}$ are single phase with the exception of $(Bi_{0.93}Zr_{0.07})_{0.85}Y_{0.15}O_{1.5+\delta}$. For this sample, the XRD pattern exhibit an additional reflection that corresponds to an interplanar spacing of $d = 0.300$ nm. This reflection may be ascribed to a 100% peak of the zirconium dioxide phase (for instance, [29]). Only reflections of the phase isostructural to δ-Bi_2O_3 were observed in the X-ray diffraction patterns of other oxides. The parameters of the face-centered cubic (f.c.c.) unit cell of the solid solutions are listed in Table 1. The unit cell volume decreases regularly with increasing dopant concentration, which is characteristic of stabilized δ-Bi_2O_3 [15–17].

Although XRD analysis of $(Bi_{0.92}Nb_{0.08})_{0.95}Ho_{0.05}O_{1.5+\delta}$ indicated an absence of phase impurities, DTA studies of this oxide in heating regime showed an endothermic effect at 814 $\pm$ 1 K. No thermal effects were observed for other prepared ceramics in the temperature range 300–1120 K. This suggests that the dopant content in $(Bi_{0.92}Nb_{0.08})_{0.95}Ho_{0.05}O_{1.5+\delta}$ is insufficient to stabilize completely the δ-phase of Bi_2O_3, which is in agreement with our data on the Bi_2O_3–Nb_2O_5 system reported in the first part of the present paper.

Annealing of the specimens in air at temperatures below 900 K results in partial decomposition of the

Table 1 Properties of the Bi_2O_3-based ceramics. ρ_{exp}, density of ceramics; ρ_{theor}, theoretical value of the density calculated from the XRD data; $\bar{\alpha}$, thermal expansion coefficient calculated from dilatometric data and averaged in the given temperature range

Composition	ρ_{exp}, kg/m^3	$\frac{\rho_{exp}}{\rho_{theor}}$, %	Parameter of the unit cell, a, nm	Mean values of thermal expansion coefficient	
			($\pm$ 0.0001 nm)	T, K	$\bar{\alpha} \cdot 10^6$, K^{-1}
$(Bi_{0.95}Nb_{0.05})_{0.90}Ho_{0.10}O_{1.5+\delta}$	7680	87	0.5525	340–690	13.3 $\pm$ 0.8
				690–1030	24 $\pm$ 1
$(Bi_{0.95}Nb_{0.05})_{0.85}Ho_{0.15}O_{1.5+\delta}$	7520	85	0.5508	330–690	13.1 $\pm$ 0.7
				690–1050	20.4 $\pm$ 0.7
$(Bi_{0.92}Nb_{0.08})_{0.95}Ho_{0.05}O_{1.5+\delta}$	7290	–	0.5523	320–700	11.8 $\pm$ 0.4
				710–1020	17.4 $\pm$ 0.9
$(Bi_{0.92}Nb_{0.08})_{0.90}Ho_{0.10}O_{1.5+\delta}$	7480	85	0.5497	340–710	12.8 $\pm$ 0.4
				710–1010	21.1 $\pm$ 0.4
$(Bi_{0.95}Zr_{0.05})_{0.85}Y_{0.15}O_{1.5+\delta}$	7580	92	0.5519	320–710	13.8 $\pm$ 0.8
				710–1120	16.6 $\pm$ 0.8
$(Bi_{0.93}Zr_{0.07})_{0.85}Y_{0.15}O_{1.5+\delta}$	7370	89	0.5515	320–680	13.3 $\pm$ 0.6
				680–1100	17.5 $\pm$ 0.9

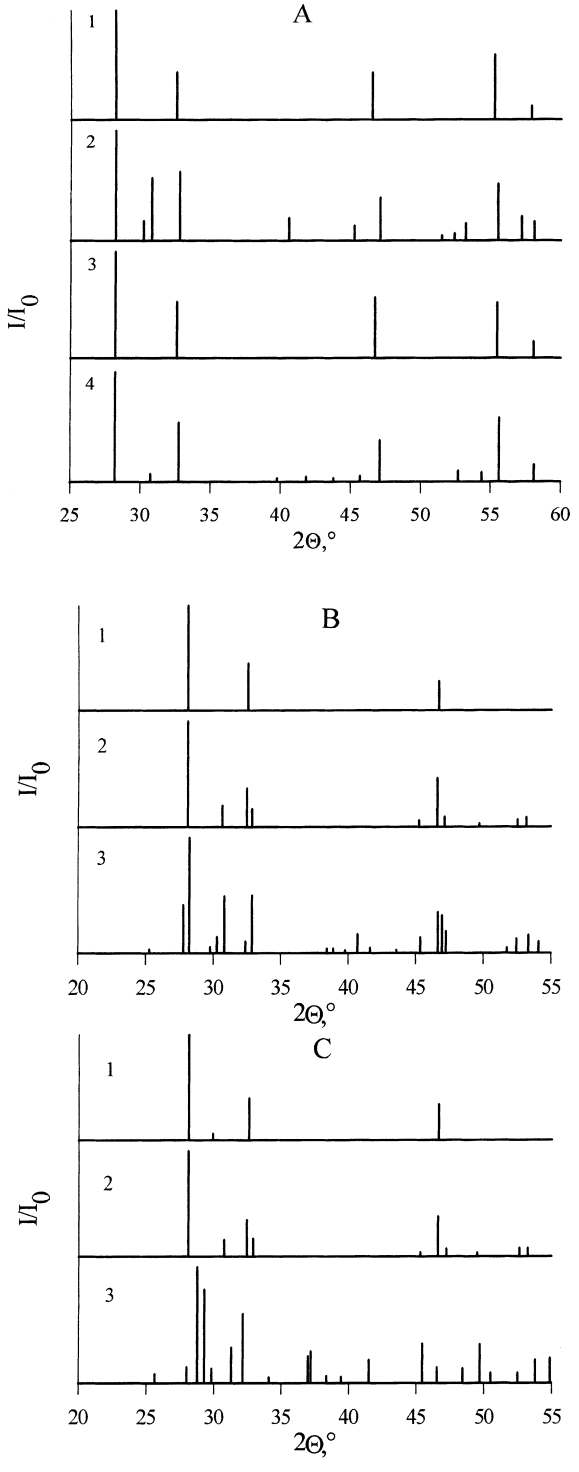

Fig. 2A–C Schematics of the initial fragments of XRD patterns (CuK_α-radiation, Ni-filter): **A** *1* As-prepared ceramics of $(Bi_{0.95}Nb_{0.05})_{0.85}Ho_{0.15}O_{1.5+\delta}$, *2* ceramics of $(Bi_{0.95}Nb_{0.05})_{0.85}Ho_{0.15}O_{1.5+\delta}$ annealed in air at 773 ± 3 K for 240 h, *3* as-prepared ceramics of $(Bi_{0.92}Nb_{0.08})_{0.90}Ho_{0.10}O_{1.5+\delta}$, *4* ceramics of $(Bi_{0.92}Nb_{0.08})_{0.90}Ho_{0.10}O_{1.5+\delta}$ annealed in air at 773 ± 3 K for 240 h. **B** The $(Bi_{0.95}Zr_{0.05})_{0.85}Y_{0.15}O_{1.5+\delta}$ ceramics: *1* after preparation, *2* after annealing in air at 873 ± 3 K for 240 h, and *3*, after annealing in air at 773 ± 3 K for 240 h. **C** The $(Bi_{0.93}Zr_{0.07})_{0.85}Y_{0.15}O_{1.5+\delta}$ ceramics: *1* after preparation, *2* after annealing in air at 873 ± 3 K for 240 h, and *3* after annealing in air at 773 ± 3 K for 240 h

δ-Bi_2O_3-like phase. New reflections, which have been observed in the XRD patterns after such annealing, were not identified. It was demonstrated that these reflections cannot be assigned to known phases on the basis of Bi_2O_3 including the phases reported in [10–14] as well as binary oxides. Figure 2 show a schematic drawing of the XRD patterns of the ceramic materials when annealed at 770 and 870 K for 240 h. Thus, the phase transformations at $T < 900$ K is characteristic of the fluorite-type solid solutions of $Bi(Nb,Ho)O_{1.5+\delta}$ and $Bi(Zr,Y)O_{1.5+\delta}$. In order to identify the nature and products of the phase decomposition, further studies are required.

Electrical conductivity of the $(Bi_{1-x}Nb_x)_{1-y}Ho_yO_{1.5+\delta}$ and $(Bi_{1-x}Zr_x)_{1-y}Y_yO_{1.5+\delta}$ ceramics correlates with the XRD and DTA data. Therefore, a decrease in the crystal lattice parameter with increasing dopant concentration is associated with decreasing conductivity (Fig. 3). Such behaviour is in agreement with the standard statement that oxygen ion mobility is a function of the geometrical dimensions of channels for the ion transfer [24, 30]. For the $(Bi_{0.92}Nb_{0.08})_{0.95}Ho_{0.05}O_{1.5+\delta}$ ceramics, the δ-phase stabilization at temperatures above 820 K results in increasing conductivity. The activation energy for electrical conductivity was calculated using the Arrhenius model [23]:

$$\sigma = \frac{A_o}{T} \cdot \exp\left[-\frac{E_a}{RT}\right] \quad (7)$$

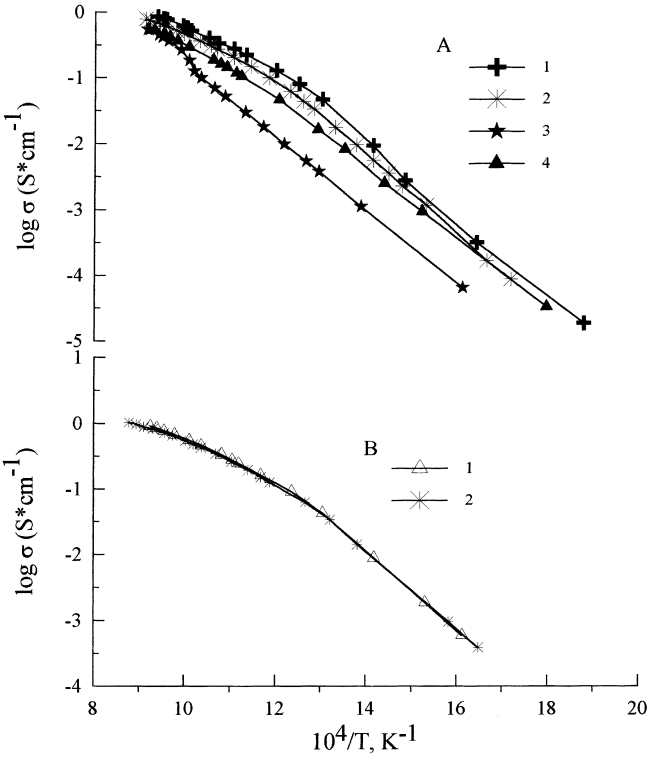

Fig. 3A, B Temperature dependence of electrical conductivity in air: **A** $(Bi_{1-x}Nb_x)_{1-y}Ho_yO_{1.5+\delta}$ ceramics with *1* $x = 0.05$, $y = 0.10$; *2* $x = 0.05$, $y = 0.15$; *3* $x = 0.08$, $y = 0.05$; *4* $x = 0.08$, $y = 0.10$. **B** $(Bi_{1-x}Zr_x)_{1-y}Y_yO_{1.5+\delta}$ ceramics with *1* $x = 0.05$, $y = 0.15$; *2* $x = 0.07$, $y = 0.15$

Table 2 Regression parameters of temperature dependence of electrical conductivity for the $(Bi_{1-x}Nb_x)_{1-y}Ho_yO_{1.5+\delta}$ ceramics in air. E_a activation energy for electrical conductivity; ρ, correlation coefficient of the regression model Eq. 7.

Composition	T, K	E_a, kJ/mol	$\ln(A_o)$ (S/m)	ρ
$(Bi_{0.95}Nb_{0.05})_{0.90}Ho_{0.10}O_{1.5+\delta}$	530–800	118 ± 6	26 ± 1	0.9987
	800–1070	70 ± 2	19.4 ± 0.3	0.9985
$(Bi_{0.95}Nb_{0.05})_{0.85}Ho_{0.15}O_{1.5+\delta}$	580–810	119 ± 1	26.3 ± 0.2	0.9998
	810–1100	73 ± 3	19.5 ± 0.4	0.9970
$(Bi_{0.92}Nb_{0.08})_{0.95}Ho_{0.05}O_{1.5+\delta}$	620–1100	117 ± 2	23.8 ± 0.3	0.9990
$(Bi_{0.92}Nb_{0.08})_{0.90}Ho_{0.10}O_{1.5+\delta}$	560–830	108 ± 2	23.9 ± 0.3	0.9999
	830–1080	81 ± 3	20.1 ± 0.3	0.9990
$(Bi_{0.95}Zr_{0.05})_{0.85}Y_{0.15}O_{1.5+\delta}$	540–810	120 ± 2	26.9 ± 0.4	0.9998
	810–1080	69 ± 3	19.2 ± 0.3	0.9980
$(Bi_{0.93}Zr_{0.07})_{0.85}Y_{0.15}O_{1.5+\delta}$	610–790	117 ± 3	26.3 ± 0.5	0.9999
	990–1140	67 ± 3	18.9 ± 0.4	0.9970

where σ is the specific electrical conductivity, A_o is the pre-exponential factor, and E_a is the activation energy. Regression parameters obtained by fitting of the experimental data are presented in Table 2. The temperature dependence of the conductivity related to the Arrhenius coordinates can be approximated by two linear segments at 530–800 K and 900–1150 K. The values of the activation energy for electrical conductivity at temperatures below 800 K are in the range 108–120 kJ mol^{-1}. Increasing temperature leads to a decrease in the activation energy to 67–81 kJ mol^{-1}.

Annealing of the Bi(Nb,Ho)$O_{1.5+\delta}$ and Bi(Zr,Y)-$O_{1.5+\delta}$ ceramics at temperatures below 900 K in air was ascertained to result in a sharp decrease in conductivity, which is caused by the phase decomposition. Thus, the conductivity decreases by a factor of 3–30 after annealing at 770–870 K for 200–240. Time dependence of the conductivity can be adequately approximated by the empirical equation [13]

$$\sigma(t) = \sigma_{t=\infty} + (\sigma_{t=0} - \sigma_{t=\infty}) \exp\left[-\left(\frac{t}{\tau_{dec}}\right)^{m_o}\right] \quad (8)$$

where $\sigma_{t=0}$ is the initial conductivity, $\sigma_{t=\infty}$ is the conductivity after infinite time, τ_{dec} is the pertinent time constant which represents a rate of the conductivity degradation, and m_0 is a dimensionless parameter. Experimental points on the time dependence of the conductivity are entered on Fig. 4. The fitting results obtained using the regression model of Eq. 8 are plotted in Fig. 4 as the solid lines. Calculated regression parameters of the model are given in Table 3. The rate of

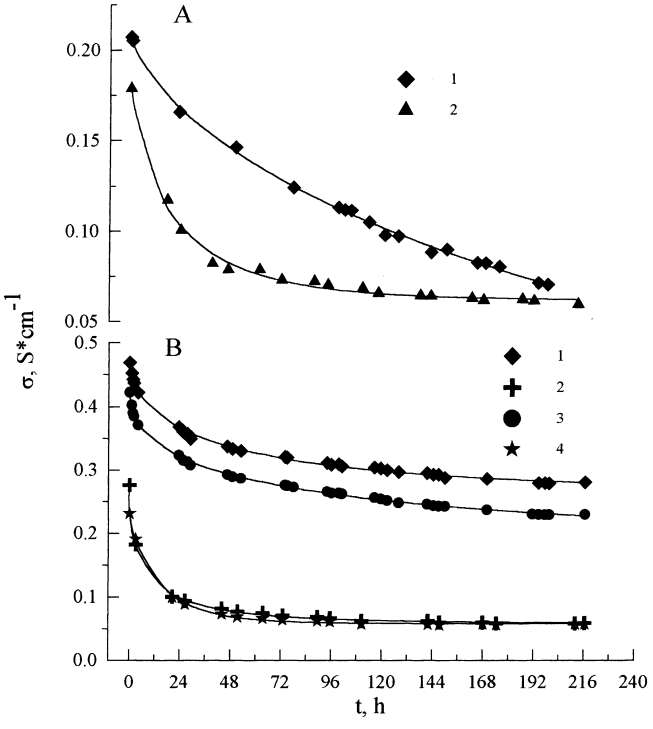

Fig. 4A, B Time dependence of electrical conductivity in air: **A** *1* $(Bi_{0.95}Nb_{0.05})_{0.85}Ho_{0.15}O_{1.5+\delta}$ at 773 ± 3 K, *2* $(Bi_{0.92}Nb_{0.08})_{0.90}Ho_{0.10}$ $O_{1.5+\delta}$ at 773 ± 3 K. **B** *1* $(Bi_{0.95}Zr_{0.05})_{0.85}Y_{0.15}O_{1.5+\delta}$ at 873 ± 3 K, *2* $(Bi_{0.93}Zr_{0.07})_{0.85}Y_{0.15}O_{1.5+\delta}$ at 873 ± 3 K, *3* $(Bi_{0.95}Zr_{0.05})_{0.85}Y_{0.15}$ $O_{1.5+\delta}$ at 773 ± 3 K, and *4* $(Bi_{0.93}Zr_{0.07})_{0.85}$ $Y_{0.15}O_{1.5+\delta}$ at 773± 3 K. The *solid lines* correspond to the fitting results

Table 3 Regression parameters of the time dependence of electrical conductivity. ρ is the correlation coefficient of the regression model Eq. 8

Composition	T, K	$\sigma_{t=0}$	Coefficients of the regression model Eq. 8			Fitting parameters	
		S/cm	$\sigma_{t=\infty}$, S/cm	τ_{dec}, h	m_0	ρ	Relative error, %
$(Bi_{0.95}Nb_{0.05})_{0.85}Ho_{0.15}O_{1.5+\delta}$	773	0.207	–0.09[1]	395	0.68	0.9991	0.9
$(Bi_{0.92}Nb_{0.08})_{0.90}Ho_{0.10}O_{1.5+\delta}$	773	0.179	0.061	22.4	0.736	0.9963	1.5
$(Bi_{0.95}Zr_{0.05})_{0.85}Y_{0.15}O_{1.5+\delta}$	773	0.27	0.058	8.78	0.51	0.9995	0.7
	873	0.46	0.258	48.5	0.56	0.9991	0.7
$(Bi_{0.93}Zr_{0.07})_{0.85}Y_{0.15}O_{1.5+\delta}$	773	0.23	0.058	14.2	0.82	0.9993	0.9
	873	0.42	0.168	96.6	0.476	0.9991	0.6

[1]The calculated negative value of $\sigma_{t=\infty}$ is caused by an insufficient range of the measurement time

conductivity decay was demonstrated to be significantly less in the case of the $Bi(Nb,Ho)O_{1.5+\delta}$ and $Bi(Zr,Y)O_{1.5+\delta}$ ceramics than in the case of δ-Bi_2O_3-based materials from [13]. Here, the introduction of zirconium cations into the bismuth oxide lattice is observed not to suppress the degradation. The kinetics of the conductivity decay of $Bi(Zr,Y)O_{1.5+\delta}$ is faster than that of $Bi(Nb,Ho)O_{1.5+\delta}$. Because of the degradation of the conductivity, the ceramic materials studied can be used for electrochemical cells such as oxygen separators only at temperatures above 950 K.

According to the results of the transference number measurements, the conductivity of the $(Bi_{1-x}Nb_x)_{1-y}Ho_yO_{1.5+\delta}$ and $(Bi_{1-x}Zr_x)_{1-y}Y_yO_{1.5+\delta}$ solid solutions is predominantly ionic. At the oxygen/air gradients, the electronic conductivity was determined by the e.m.f. method to be less than 10% of the total conductivity of the materials (Table 4). Decreasing oxygen partial pressure leads to decreasing ion transference numbers, which is caused by oxygen leaving the crystal lattice and increasing electronic conductivity. Such results are typical of oxides on the basis of δ-Bi_2O_3. One can also note a tendency for a decrease in electron transference numbers with increasing dopant content within the studied concentration range. Table 5 presents the ion transference numbers calculated from the Faradaic efficiency measurements of the $(Bi_{0.95}Zr_{0.05})_{0.85}Y_{0.15}O_{1.5+\delta}$ and $Zr_{0.90}Y_{0.10}O_{1.95}$ ceramics. The YSZ specimen was investigated in order to verify the measurement technique. Within the limits of experimental error, the results of the Faradaic efficiency studies of $(Bi_{0.95}Zr_{0.05})_{0.85}Y_{0.15}O_{1.5+\delta}$ are coincident with the e.m.f. data. Attempts to measure Faradaic efficiency at lower temperatures have not met with success, due to increasing resistance of the electrolyte specimens with time (Fig. 4).

Thermal expansion coefficients (TECs) of the ceramics listed in Table 1 were calculated from the dilatometric data and averaged in the given temperature ranges. The dilatometric curves of the $Bi(Nb,Ho)O_{1.5+\delta}$ ceramics are shown in Fig. 5. One should note a correlation between the ionic conductivity and thermal expansion, which is characteristic of oxygen ion-conducting materials [17, 24, 31]. According to the phenomenological theory of ionic transport [24], the

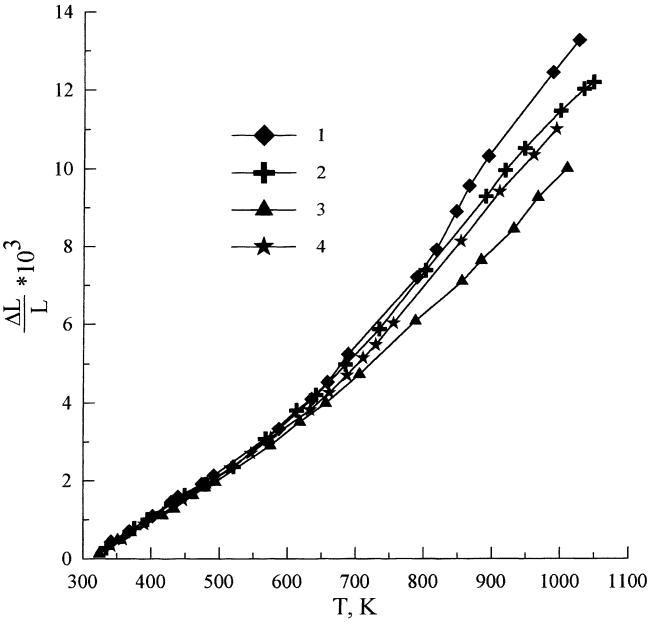

Fig. 5. Thermal expansion of the $(Bi_{1-x}Nb_x)_{1-y}Ho_yO_{1.5+\delta}$ ceramics in air: *1* $x = 0.05$, $y = 0.10$; *2* $x = 0.05, y = 0.15$; *3* $x = 0.08, y = 0.05$, *4* $x = 0.08$, $y = 0.10$

Table 4 Oxygen ion transference numbers of the $(Bi_{1-x}Nb_x)_{1-y}$ $Ho_yO_{1.5+\delta}$ ceramics determined by the e.m.f. method[1]

Composition	T, K	Cell	t_o
$(Bi_{0.95}Nb_{0.05})_{0.90}Ho_{0.10}O_{1.5+\delta}$	973	1	0.95 ± 0.01
$(Bi_{0.95}Nb_{0.05})_{0.85}Ho_{0.15}O_{1.5+\delta}$	973	1	0.96 ± 0.01
	928	1	0.96 ± 0.01
	882	1	0.98 ± 0.01
	973	2	0.90 ± 0.02
$(Bi_{0.92}Nb_{0.08})_{0.90}Ho_{0.10}O_{1.5+\delta}$	973	1	0.96 ± 0.01
$(Bi_{0.95}Zr_{0.05})_{0.85}Y_{0.15}O_{1.5+\delta}$	883	1	0.95 ± 0.01
	798	1	0.92 ± 0.02
	751	1	0.91 ± 0.08
$(Bi_{0.93}Zr_{0.07})_{0.85}Y_{0.15}O_{1.5+\delta}$	908	1	0.96 ± 0.02
	883	1	0.96 ± 0.01
	798	1	0.99 ± 0.02

[1]The table contains the ion transference number values and their errors calculated according to [17]

Table 5 Oxygen ion transference numbers in air determined from the Faradaic efficiency measurements

Composition	T, K	t_o	Current density, mA cm^{-2}	Voltage, mV	ρ[1]
$(Bi_{0.95}Zr_{0.05})_{0.85}Y_{0.15}O_{1.5+\delta}$	973	0.93 ± 0.03	85	270–405	0.9996
	973	0.91 ± 0.03	124	385–535	0.9997
$Zr_{0.90}Y_{0.10}O_{1.95}$	1073	1.02 ± 0.03	102	1140–1175	0.9997
	973	1.02 ± 0.03	64	1190–1260	0.9995

[1]ρ is the correlation coefficient of the regression model Eq. 6

relationship between TEC and ionic conductivity is due to the increasing mobility of point defects responsible for the ionic transport with thermal expansion of the crystal. Analogous correlation has been mentioned earlier for $Bi(Pb,Y)O_{1.5+\delta}$ fluorite-type solid solutions and $SrCo(Ti)O_{3-\delta}$ perovskites [17, 31].

Conclusions

1. Fluorite-type solid solutions of $(Bi_{1-x}Nb_x)_{1-y}Ho_yO_{1.5+\delta}$ ($x = 0.05$ and 0.08; $y = 0.10 - 0.15$) and $(Bi_{1-x}Zr_x)_{1-y}Y_yO_{1.5+\delta}$ ($x = 0.05$ and 0.07; $y = 0.15$) have been prepared. Electrical conductivity, cubic unit cell volume and thermal expansion of the oxides have been found to decrease with increasing dopant content. The values of the activation energy for electrical conductivity are 108–120 kJ mol^{-1} at temperatures of 500–800 K and 67–87 kJ mol^{-1} at 800–1150 K. Thermal expansion coefficients of the ceramics lie in the range $(11.8–13.8) \times 10^{-6}$ K^{-1} at 300–700 K and $(16.6–24.0) \times 10^{-6}$ K^{-1} at 700–1100 K. Oxygen ion transference numbers have been determined by the e.m.f. method and Faradaic efficiency measurement to exceed 0.9.
2. Annealing at temperatures below 900 K leads to a phase decomposition and to a sharp decrease in conductivity of the ceramics. Additions of zirconia do not suppress the degradation. The conductivity degradation prevents use of the $Bi(Nb,Ho)O_{1.5+\delta}$ and $Bi(Zr,Y)O_{1.5+\delta}$ ceramics as materials for oxygen separators at $T < 900$ K.
3. A new technique for the study of Faradaic efficiency has been proposed. The technique has been verified using $(Bi_{0.95}Zr_{0.05})_{0.85}Y_{0.15}O_{1.5+\delta}$ and $Zr_{0.90}Y_{0.10}O_{1.95}$ ceramic samples. Within the limits of experimental error, the results of the Faradaic efficiency studies coincide with the e.m.f. data.

References

1. Bouwmeester HJM, Burgraaf AJ (1996) In: Burgraaf AJ, Cot L (eds) Fundamentals of inorganic membrane science and technology. Elsevier, Amsterdam, pp 435–528
2. Mazanec TJ (1994) Solid State Ionics 70/71: 11
3. Wu Z, Liu M (1997) Solid State Ionics 93: 65
4. Kharton VV, Zhuk PP, Naumovich EN, Vecher AA, Tonoyan AA (1991) USSR Patent 1794931
5. Mazanec TJ, Velenyi LJ (1992) US Patent 5160713
6. Liu M, Joshi AV, Shen Y, Krist K (1993) US Patent 5273628
7. Shen Y, Joshi AV, Krist K, Liu M, Virkar AV (1997) US Patent 5616223
8. Balagopal S, Boettcher M, Cutler RA, Taylor D, Hu H, Namjoshi S, Liu M (1995) Annual Report for Gas Research Institute under Contract No. 5092-260-2487
9. Shen Y, Joshi A, Liu M, Krist K (1994) Solid State Ionics 72: 209
10. Zhow W, Jefferson DA, Thomas JM (1986) Proc R Soc London, Ser A 406: 173
11. Zhow W, Jefferson DA, Thomas JM (1987) J Solid State Chem 70: 129
12. Fung KZ, Virkar AV, Drobeck DL (1994) J Am Ceram Soc 77: 1638
13. Fung KZ, Chen J, Virkar AV (1993) J Am Ceram Soc 76: 2403
14. Huang K, Feng M, Goodenough JB (1996) Solid State Ionics 89: 17
15. Kharton VV, Naumovich EN (1993) Russian J Electrochem 29: 1297
16. Naumovich EN (1991) Thesis. Belarus State University, Minsk, Belarus [in Russian]
17. Naumovich EN, Skilkov SA, Kharton VV, Tonoyan AA, Vecher AA (1994) Russian J Electrochem 30: 642
18. Kharton VV, Naumovich EN, Zhuk PP, Demin AK, Nikolaev AV (1992) Russian J Electrochem 28: 1376
19. Kharton VV, Naumovich EN, Samokhval VV (1997) Solid State Ionics 99: 269
20. Kharton VV, Naumovich EN, Vecher AA, Nikolaev AV (1995) J Solid State Chem 120: 128
21. Kovalevsky AV, Kharton VV, Naumovich EN (1996) Inorganic Mater 32: 1230
22. Gorelov VP (1988) Elektrokhimiya 24: 1380 [in Russian]
23. Rickert H (1982) Electrochemistry of solids. An introduction. Springer, Berlin Heidelberg New York
24. Chebotin VN (1982) Physical chemistry of solids. Khimiya, Moscow [in Russian]
25. Fabry P, Kleitz M, Deportes C (1972) J Solid State Chem 5: 1
26. Iharada T, Hammouche A, Fouletier J, Kleitz M, Boivin JC, Mairesse G (1991) Solid State Ionics 48: 257
27. Kharton VV, Viskup AP, Naumovich EN, Lapchuk NM (1997) Solid State Ionics 104: 67
28. Haase R (1963) Thermodynamik der Irreversiblen Prozesse. Dr Dietrich Steinkopff Darmstadt [in German]
29. Powder Diffraction Files, card No 24-1164
30. Verkerk MJ, Burgraaf AJ (1981) Solid State Ionics 3: 463
31. Kharton VV, Shuangbao Li, Kovalevsky AV, Naumovich EN (1997) Solid State Ionics 96: 141